J|A|C|S ARTICLES

Published on Web 08/05/2009

Electric Bistability in Pentacene Film-Based Transistor Embedding Gold Nanoparticles

Chiao-Wei Tseng[†] and Yu-Tai Tao*[,†,‡]

Institute of Chemistry, Academia Sinica, Taipei, Taiwan, Republic of China 115 and Department of Chemistry, National Tsing-Hua University, Hsinchu, Taiwan, Republic of China, 115

Received June 22, 2009; E-mail: ytt@chem.sinica.edu.tw

Abstract: Pentacene films were deposited on a silica surface decorated with gold nanoparticles (Au-NPs). The crystallinity and packing orientation of the film are critically dependent on the surface properties of the nanoparticles, which can be tuned by a self-assembled monolayer (SAM) of organic thiolate on the nanoparticles. High-performance field-effect transistors based on the Au-NPs-embedded pentacene films can be prepared if the nanoparticles are made "hydrophobic" as well as "oleophobic" by appropriate SAMs. Electrical bistability was observed in these devices, with a memory window that depends on the size and surface modification of the Au-NPs. The structural characterization and electronic characteristics of the devices will be detailed.

Introduction

Organic materials have attracted much attention for building various electronic devices because of the potential advantages of low-cost fabrication, being lightweight, and flexibility that organic materials can offer.[1] Various components are needed in electronic devices: displays, transistors, memories, switches, etc. Efforts have been devoted to incorporate organic materials into all of these components. Organic memory devices have been demonstrated in which metal nanoparticles were incorporated into a semiconducting organic layer, forming an organic/metal nanoclusters/organic (OMO) structure to create an electric bistability state in a diode consuration.[2] Trapping of charges at the nanoparticles has been proposed as one possible mechanism.[3,4] Examples of integrating an organic field-effect transistor (OFET) with a memory element were also demonstrated by doping molecular donor molecules into the insulating dielectrics of a polymer-based field-effect transistor.[5] The donor molecules serve to trap the hole charges induced in the channel region of the transistor near the interface. Integration of the transistor device with a memory element is attractive in adding another degree of freedom, the gate voltage, in controlling the memory function. It also will simplify the device architecture.

In this study, we report the incorporation of gold nanoparticles (Au-NPs) into the conducting channel of a pentacene film-based FET and the $I-V$ characteristics thereafter. Pentacene is a well-studied and promising transistor material which forms layered crystalline films upon thermal deposition on silicon substrate. The field-effect mobility through the pentacene layer highly depends on the crystallinity as well as the morphology of the film.[6] The presence of Au-NPs was shown in this work to dramatically influence the crystallinity and morphology of the thermally evaporated pentacene films, as a result of the strong metal−pentacene interfacial interaction. The interaction can, nevertheless, well be modulated by a self-assembled monolayer (SAM) of organic thiolate on the surfaces of Au-NPs. Efficient transistors can be obtained only if the Au-NPs are made "oleophobic" through the SAM adsorption. In addition, the structure of the thiol molecule used also controls the charge trapping/storing properties of the NPs through the gold work function modulation and the tunneling barrier imposed by the insulating hydrocarbon chains. Electric bistability,[7,8] that is, hysteresis in source/drain current as a function of applied gate voltage, was observed due to the charge-trapping Au-NPs. The feasibility for these Au-NPs to serve as a floating gate in the transistor/memory function is demonstrated.

Experimental Section

The pentacene-based FET was fabricated by physical vapor deposition (in a vacuum of 2×10^{-5} Torr at a deposition rate of 0.2 Å/s) of a 60 nm pentacene film on an *n*-type silicon (100) substrate (the gate electrode) which was covered with a 300 nm thick, thermally grown oxide layer as the insulating dielectric. Source and drain electrodes were deposited through a shadow mask to achieve a top-contact FET device with a channel length of 50 μm and a channel width of 500 μm. For the Au-NPs-embedded pentacene films, the oxide-covered silicon (silica) substrate was first treated with 3-mercaptopropyltrimethoxysilane, which served as the adhesion layer for Au-NPs.[9] Au-NPs were prepared by depositing gold at a rate of 0.1 Å/s on the surface to various thicknesses.

[†] National Tsing-Hua University.
[‡] Academia Sinica.

(1) Dimitrakopoulos, C. D.; Malenfant, P. R. L. *Adv. Mater.* **2002**, *14*, 99.
(2) Yang, Y.; Ouyang, J.; Ma, L. P.; Tseng, R. J. H.; Chu, C. W. *Adv. Funct. Mater.* **2006**, *16*, 1001–1014.
(3) Scott, J. C.; Bozano, L. D. *Adv. Mater.* **2007**, *19*, 1452–1463.
(4) Bozano, L. D.; Kean, B. W.; Beinhoff, B.; Carter, K. R.; Rice, P. M.; Scott, J. C. *Adv. Funct. Mater.* **2005**, *15*, 1933–1939.
(5) Wu, W.; Zhang, H.; Wang, Y.; Ye, S.; Guo, Y.; Di, C.; Yu, G.; Zhu, D.; Liu, Y. *Adv. Funct. Mater.* **2008**, *18*, 2593–2610.
(6) Lee, H. S.; Kim, D. H.; Cho, J. H.; Hwang, M.; Jang, Y.; Cho, K. *J. Am. Chem. Soc.* **2008**, *130*, 10556–10564.
(7) Ma, L. P.; Liu, J.; Yang, Y. *Appl. Phys. Lett.* **2002**, *80*, 2997.
(8) Ma, L. P.; Liu, J.; Pyo, S.; Yang, Y. *Appl. Phys. Lett.* **2002**, *80*, 362.
(9) Love, J. C.; Estroff, L. A.; Kriebel, J. K.; Nuzzo, R. G.; Whitesides, G. M. *Chem. Rev.* **2005**, *105*, 1103–1169.

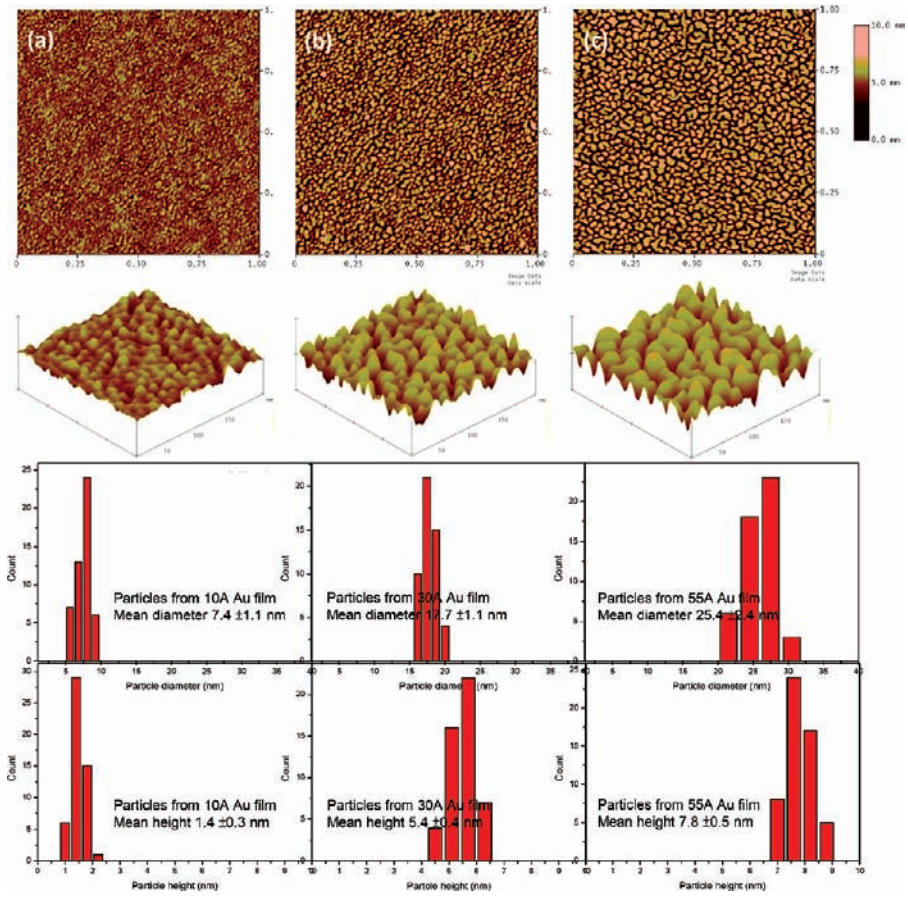

Figure 1. AFM micrographs and corresponding histograms of Au-NPs prepared by thermal evaporation to a nominal thickness of (a) 1, (b) 3, and (c) 5.5 nm.

Additional cleaning by low-power oxygen plasma for 5 min was carried out to clean off both the silica and the Au-NPs surfaces. These nanoparticle-decorated substrates were used immediately for pentacene deposition or immersed in a 1 mM ethanol solution of thiol molecules for 12 h for SAM formation and then thoroughly rinsed with pure ethanol before the pentacene film deposition. *n*-Alkanethiol ($CH_3(CH_2)_nSH$, $n = 5, 7, 11, 17$) and fluorinated thiols ($CF_3(CF_2)_nCH_2CH_2SH$, $n = 3, 5, 7$) were obtained commercially. ω-Mercaptoalkanoic acids, benzylmercaptan, and 2,6-difluorobenzylmercaptan were synthesized in the laboratory. Atomic force microscope analyses were carried out with a Multimode Atomic Force Microscope (Digital Instruments, Nanoscope III) using tapping mode with a silicon tip. The powder X-ray diffraction measurement was carried out by using the Philips X′Pert diffractometer equipped with an X′Celerator detector. The electrical characteristics of the transistor devices were measured in ambient with a HP4156 parameter analyzer.

Results and Discussion

Film Structure Characterization. The gold nanoparticles were prepared by evaporating pure gold metal onto the silica substrate. To improve the adhesion of gold to the surface, the silica substrate was pretreated with 3-mercaptopropyltrimethoxysilane to form a thiol-functionalized surface.[8] Figure 1 shows AFM micrographs of the gold films with a nominal thickness of 1, 3, and 5.5 nm and their histograms. As can be seen, discrete particles were obtained at all these thicknesses. At a nominal thickness of 1 nm, the average size of the Au-NPs is ~1.5 nm in height and ~7.8 nm in diameter. The size increases with increasing nominal thickness to ~5.7 nm in height and ~19.1 nm in diameter for the 3 nm film and to ~7.3 nm in height and ~24 nm in diameter for the 5.5 nm film. The anchored Au-NPs are stable to plasma cleaning and solvent wash. Plasma treatment and SAM adsorption had little effect on the size of the particles, except a slight decrease of rms roughness. With the standard FET device configuration, the conductivity of the Au-NPs-covered silica is slightly higher than the silica itself (current increases from ~0.1 to ~1 nA). The capping of Au-NPs with SAM, however, decreases the conductivity (to ~0.01 nA). Compared to the conductivity measured for the pentacene-film based devices (current $\sim 10^{-4}-10^{-5}$A), the presence of Au-NPs has a negligible contribution to the conductivity observed for the pentacene film-based FET devices.

Pentacene films were deposited at a substrate temperature of 24 °C. Figure 2a shows the X-ray diffraction patterns for 60 nm pentacene films on the silica surfaces decorated with unmodified or various *n*-alkanethiol-modified Au-NPs (designated as C*n*-Au-NPs, $n = 6, 8, 12, 18$) obtained from 3 nm Au film. Characteristic diffraction peaks appeared at $2\theta = 5.8°$, 11.5°, 17.3°, and 23.1° on all substrates, assignable to the (001), (002), (003), and (004) diffraction peaks, respectively, for the thin film phase of pentacene.[10,11] These results indicate that pentacene films on the Au-NPs-decorated silica surface have the expected layered and herringbone packing with the long molecular axes aligning nearly perpendicular to the substrate. However, there is a distinct

(10) Weng, S. Z.; Hu, W. S.; Kuo, C. H.; Tao, Y. T.; Fan, L. J.; Yang, Y. W. *Appl. Phys. Lett.* **2006**, *89*, 172103.
(11) Hu, W. S.; Tao, Y. T.; Hsu, Y. J.; Wei, D. H.; Wu, Y. S. *Langmuir* **2005**, *21*, 2260–2266.

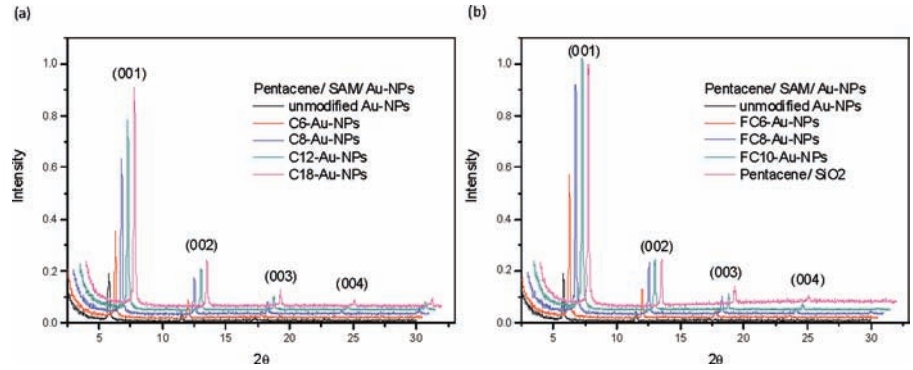

Figure 2. X-ray diffraction patterns for the 60 nm thick pentacene films deposited on (a) *n*-alkanethiol (C*n*SH, $n = 6, 8, 12, 18$) modified Au-NPs/silica and (b) fluorinated thiol (FC*n*SH, $n = 6, 8, 10$) modified Au-NPs/silica surface. The data include pentacene films deposited on the unmodified Au-NPs/silica and bare silica surface.

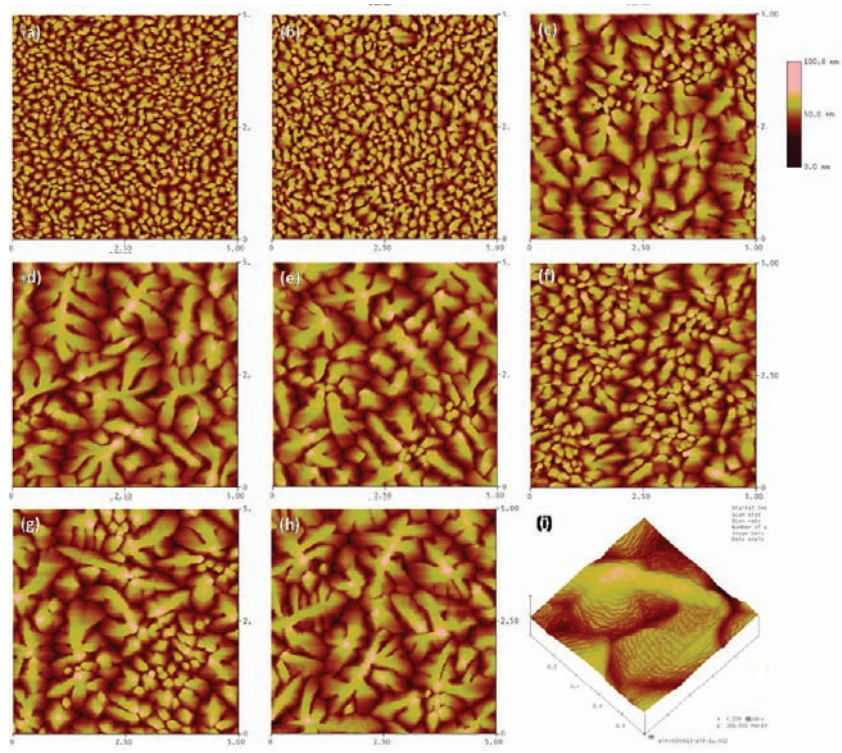

Figure 3. AFM images of pentacene films deposited on various substrates: (a) unmodified Au-NPs/silica, (b−e) *n*-alkanethiol (C*n*, $n = 6, 8, 12, 18$) modified Au-NPs/silica, (f−h) fluorinated alkanethiol (FC*n*, $n = 6, 8, 10$) modified Au-NPs/silica. All images are 5 μm × 5 μm in size and 100 nm in height scale. (i) Three-dimensional AFM image of the pentacene films on FC10-Au-NPs/silica. The image is 1 μm × 1 μm in size.

trend in the intensity of the diffraction peaks: lowest on the substrate with unmodified Au-NPs and increases with increasing chain length of the thiol used for SAM modification on Au-NPs.

Similar film deposition was carried out on substrates with Au-NPs modified with fluorinated *n*-alkanethiols of various chain lengths (designated as FC*n*-Au-NPs, $n = 6, 8, 10$). The X-ray diffraction measurements are shown in Figure 2b. Again, a dependence of diffraction peak intensity with the chain length was observed. With FC10-Au-NPs on the silica substrate, the intensity reaches that for pentacene film deposited on a bare silica surface without Au-NPs on top.

The morphologies of the pentacene films on various surfaces were also examined by AFM, and the images are shown in Figure 3. The pentacene films deposited on substrates with unmodified Au-NPs and with C6-Au-NPs apparently exhibited smaller grain sizes, ranging from 0.1 to 0.2 μm in diameter. As the chain length of the thiol increases, the average grain size increased as well, with typical dendritic crystallites as that deposited on a clean silica surface. This is in accord with the trend exhibited by the X-ray diffraction intensity in that the longer the chain length of the thiol, the higher the crystallinity of the deposited film. The trend of increasing grain sizes with increasing chain length also exists for the fluorinated nanoparticles. With the

Table 1. RMS Roughness of 5 and 10 nm Pentacene Films Deposited on Various Substrates

	Au surface rms (nm)	pentacene/ unmodified Au rms (nm)	pentacene/C6-Au rms (nm)	pentacene/ C12-Au rms (nm)	pentacene/ C18-Au rms (nm)
pentacene (5 nm)/ SAM/Au-NPs	1.4	5.7	4.4	2.8	2.7
pentacene (10 nm)/ SAM/Au-NPs	1.3	7.8	4.7	3.2	3.1
pentacene (10 nm)/ SAM/Au-film	1.5	4.1	3.6	3.3	3.3

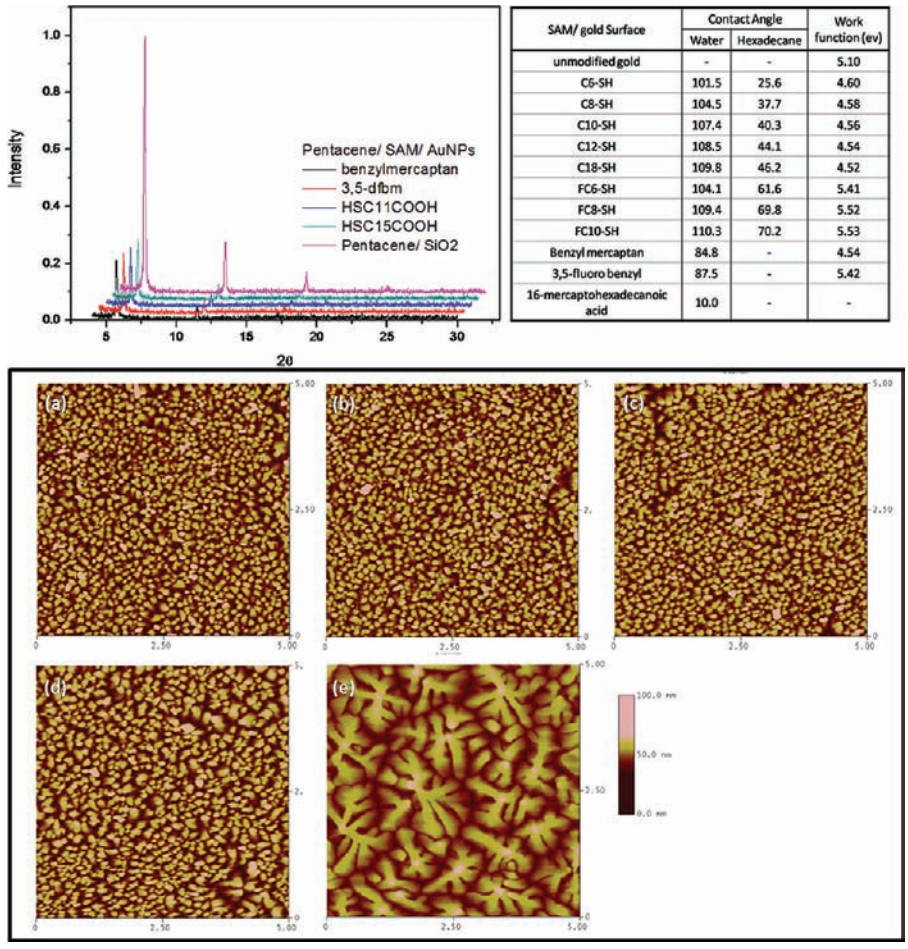

SAM/ gold Surface	Contact Angle		Work function (ev)
	Water	Hexadecane	
unmodified gold	-	-	5.10
C6-SH	101.5	25.6	4.60
C8-SH	104.5	37.7	4.58
C10-SH	107.4	40.3	4.56
C12-SH	108.5	44.1	4.54
C18-SH	109.8	46.2	4.52
FC6-SH	104.1	61.6	5.41
FC8-SH	109.4	69.8	5.52
FC10-SH	110.3	70.2	5.53
Benzyl mercaptan	84.8	-	4.54
3,5-fluoro benzyl	87.5	-	5.42
16-mercaptohexadecanoic acid	10.0	-	-

Figure 4. X-ray diffraction patterns and AFM images of 60 nm thick pentacene films deposited on (a) benzylmercaptan-Au-NPs, (b) 2,6-difluorobenzylmercaptan-Au-NPs, (c) 12-mercaptododecanoic acid-Au-NPs, (d) 16-mercaptohexadecanoic acid-Au-NPs, and (e) silica. The inset table shows the contact angle and work function of gold surfaces modified with the corresponding SAMs.

same chain length of C6, fluorinated thiol-modified Au-NPs resulted in larger grains than *n*-alkanethiol-modified particles.

In an earlier work, we demonstrated that pentacene molecules deposited on a clean gold surface tend to form crystallites where the long molecular axes lie parallel to the substrate due to the strong interaction between the π cloud of the pentacene and the gold surface, whereas those deposited on *n*-alkanethiol-covered gold substrates tend to form crystallites where the long molecular axes are oriented nearly straight-up at the substrate.[11] It was suggested that the SAMs of *n*-alkanethiol generate a low-energy outer surface due to the nonpolar methyl terminal group. When the chain length of the *n*-alkanethiol increases, the surface energy of the resulting SAM-modified substrate further decreases, as indicated by the contact angles for both water and hexadecane as the wetting liquid, as shown in Table 1. The higher hexadecane contact angle and thus "oleophobicity" reflects a weaker interaction between the hydrocarbon wetting liquid and the surface than the intermolecular interaction between the wetting molecules themselves. The observed trends in the film morphology and crystallinity above appear to parallel the trend in surface energy and are rationalized as follows. When pentacene molecules land on the silica substrate decorated with clean gold particles, they would adhere to the gold surface and nucleate over the nanoparticle surfaces, in addition to those landing and nucleating on the silica surface. In other words, the gold surfaces provide numerous preferred nucleation sites. Thus, the film is composed of smaller grains, with both a flat-lying molecular orientation in the crystallites grown on gold surfaces and vertically oriented molecules in crystallites grown on the silica surface region. This leads to misoriented crystallites or poorer crystallinity and thus gives a low diffraction intensity for the (00*n*) peaks in the X-ray diffraction measurement. When the Au-NPs are covered with a SAM of *n*-alkanethiol, the surface energy is reduced and the interaction of pentacene with gold surface is weakened so that pentacene molecules could migrate to the silica surface, where they nucleate and grow crystals, with perpendicular and layered packing, as typically observed on a silica surface.[12] The longer the chain is, the lower the surface energy of Au-NPs becomes and the propensity to migrate to and grow crystallites on silica region is higher and the diffraction peak intensity gets higher. Fluorinated SAMs yield surfaces of even lower energy, and thus, for the same chain length thiol, the fluorinated Au-NPs always result in higher crystallinity of pentacene films. This suggestion is further tested with several other monolayers: ω-mercaptoalkanoic acids, benzylmercaptan, and 2,6-difluorobenzylmercaptan. Contact angles with water and hexadecane as wetting liquids on gold modified with these molecules are also shown in Table 1. Carboxyl-terminated thiols render a surface both hydrophilic and "oleophilic" (contact angle for both water and hexadecane are low). Benzylmercaptan and 2,6-difluorobenzylmercaptan render a surface "hydrophobic" but "oleophilic". The pentacene films deposited on these monolayer-covered Au-NPs exhibited

(12) Fritz, S. E.; Martin, S. M.; Frisbie, C. D.; Ward, M. D.; Toney, M. F. *J. Am. Chem. Soc.* **2004**, *126*, 4084.

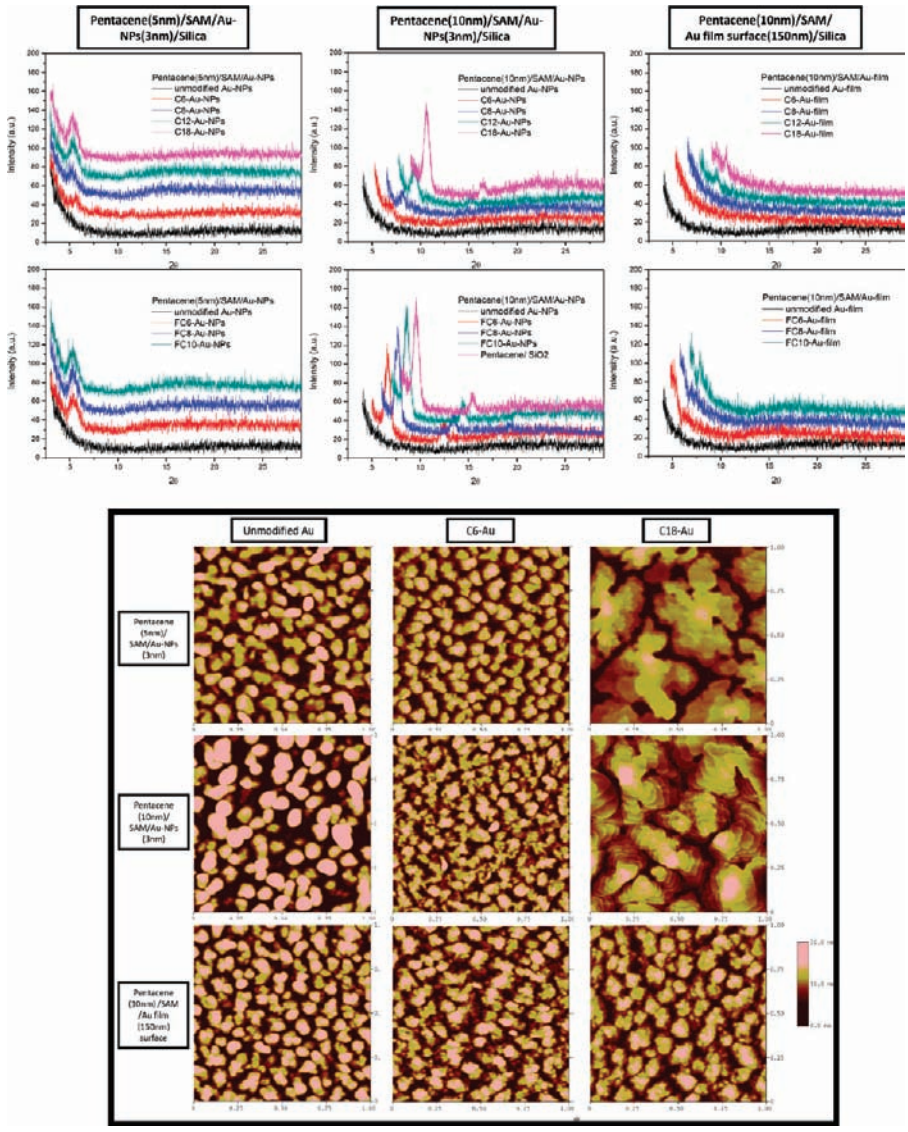

Figure 5. X-ray diffraction patterns and corresponding AFM images of 5 and 10 nm pentacene films deposited on various SAM-coated Au-NPs (from 3 nm Au layer) on silica and continuous Au film (from 150 nm Au layer), respectively.

smaller grains, as shown by AFM micrographs, and poor crystallinity, as suggested by X-ray diffraction intensity (Figure 4). Thus, the wetting property, in particular, the oleophobicity of the gold surface, plays an important role in affecting the morphology of the pentacene film deposited.

Further analyses of the surface morphology at an early stage of the deposition (5 and 10 nm) lend additional support of the suggested mechanism of film growth. AFM reveals that on substrates with unmodified Au-NPs or C6-Au-NPs, discontinuous, small, yet steep islands of pentacene were obtained with much increased surface roughness (Figure 5). Little or no signs of the (001) diffraction peak appeared at this stage. In contrast, on substrates decorated with long chain thiol (C18-Au-NPs) or fluorinated thiol-modified Au-NPs, films with layered packing and reduced roughness were obtained. The (001) diffraction peak was clearly observed even at this early stage. It is noted that the same pentacene films deposited on a flat and continuous gold film (150 nm Au deposited on a smooth silica substrate) exhibited quite different morphology and crystallinity (Figure 5). On continuous and flat Au film, smaller grains and lower crystallinity were obtained even if the Au film is covered with a C18SH SAM. The observation is explained to be due to different affinity to pentacene molecules on a composite surface of Au and silica. On clean Au-NPs-decorated silica surface, the pentacene molecules adsorb preferentially on gold surfaces and grow vertically through $\pi-\pi$ stacking to give steep piles and the roughness increases. The SAM modification on Au-NPs, particularly with long chain or fluorinated thiols, lowers the surface energy of Au-NPs and favors migration of pentacenes to silica regions and lateral growth into layered films. That is, the nucleation sites mainly reside on silica regions and film grows to fill the inter spaces between the Au-NPs. The overall roughness is thus much reduced. On a continuous Au film, there are no differentiating adsorption regions (except grain boundaries and terraces). Nucleation sites are evenly distributed and more populated than on a composite surface of Au and silica. The grains are thus smaller.

The effect of size of Au-NPs was also studied. Increasing the size of the nanoparticles (by increasing the nominal thickness of gold film from 1−3 to 5.5 nm) leads to a diminishing (001) peak intensity and smaller grain size of the pentacene films, as evidenced by X-ray and AFM in Figure 6. Increasing the gold particle size increases the ratio of gold/silica areas and also the distance for pentacene molecules to migrate from gold surfaces

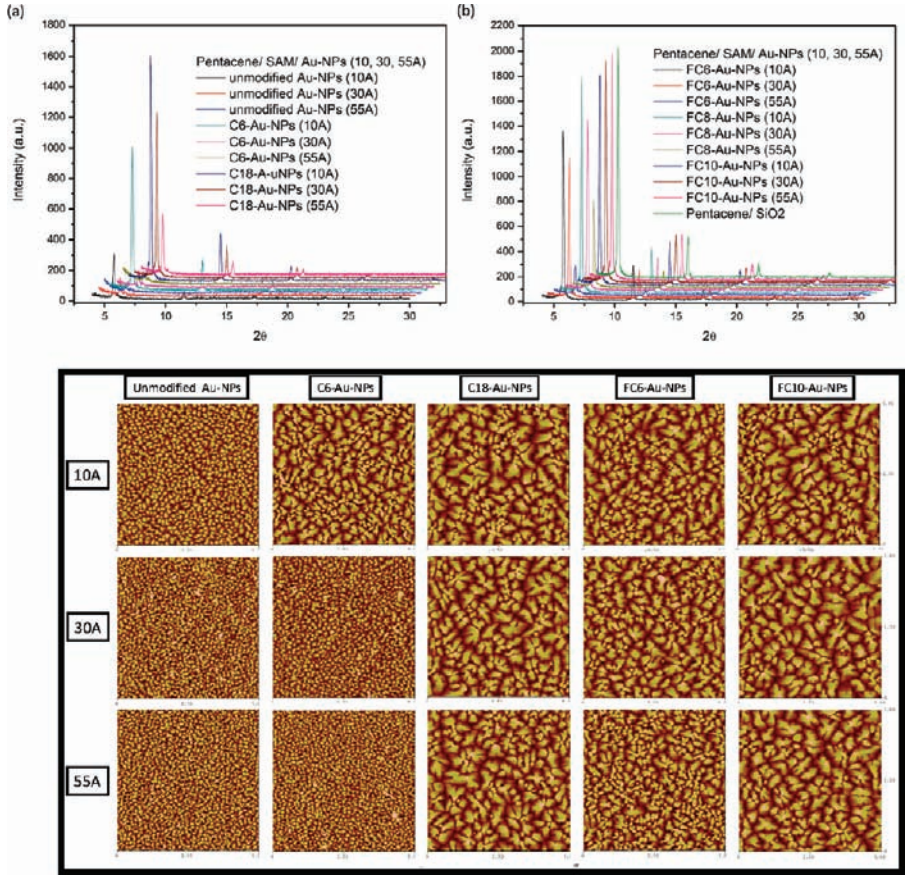

Figure 6. X-ray diffraction patterns and corresponding AFM images of the 60 nm thick pentaene films deposited on various SAM-modified Au-NPs formed from 1, 3, and 5.5 nm: (a) unmodified Au-NPs and C6- and C18-Au-NPs and (b) FC6-, FC8-, and FC10-Au-NPs and silica.

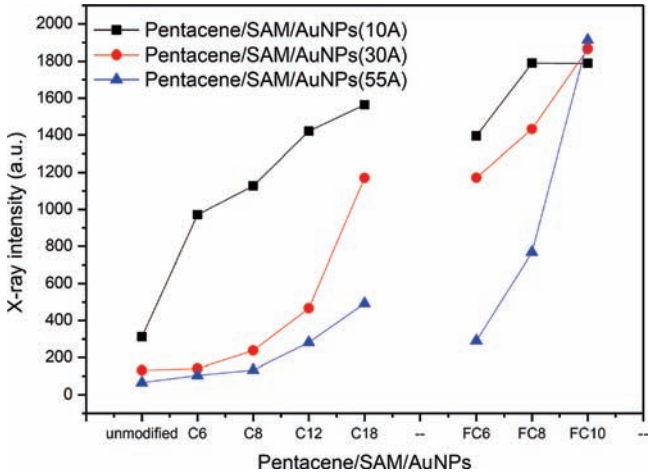

Figure 7. Correlation of the X-ray intensity of the (001) diffraction peak with chain length of SAM modifier for different sized particles.

to silica surfaces. A decrease in the amount of crystalline layers of pentacene can be rationalized. Figure 7 shows the correlation between the intensity of the (001) X-ray diffraction peak and the chain length of SAM modifiers for Au-NPs of different size. With larger nanoparticles on the substrate and thus a rougher surface, the crystallinity of deposited pentacene film is more sensitive to the chain length of SAM modification, which modulates mainly the wetting property and surface energy here. The results suggest both surface roughness and surface energy are affecting the crystallinity of the pentacene films.

On the basis of the discussion above, a summary of the proposed film growth process is shown in Scheme 1.

Scheme 1. Schematic Diagrams of the Pentacene Molecules Deposited on Silicon Substrate Decorated with (A) Unmodified Au-NPs and (b) SAM-Modified Au-NPs

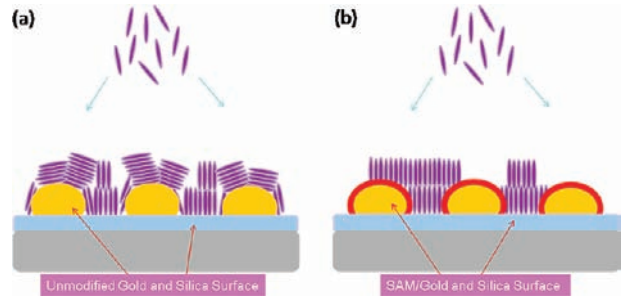

Electric Property. The electrical characteristics of the devices with Au-NPs-embedded pentacene film as channel material were measured. With unmodified Au-NPs embedded in the film, little current (as low as 3×10^{-7} A) was obtained and no field effect was observed, presumably due to the low crystallinity and/or the wrong packing orientation of pentacene crystallites.[13] With the nanoparticle surfaces modified with SAMs of *n*-alkanethiol or fluorinated *n*-alkanethiol, typical *p*-type transistor behavior was observed. The field-effect mobility, nevertheless, depends on the chain length of the thiol used and increases with increasing chain length, from 0.036 $cm^2/(V\ s)$ for C6-Au-NPs to 0.18 $cm^2/(V\ s)$ for C18-Au-NPs and from 0.17 $cm^2/(V\ s)$ for FC6-Au-NPs to 0.21 $cm^2/(V\ s)$ for FC10SH-Au-NPs. The latter value is similar to the mobility obtained in the absence of Au-

(13) Hu, W. S.; Tao, Y. T.; Chen, Y. F.; Chang, C. S. *Appl. Phys. Lett.* **2008**, *93*, 053304.

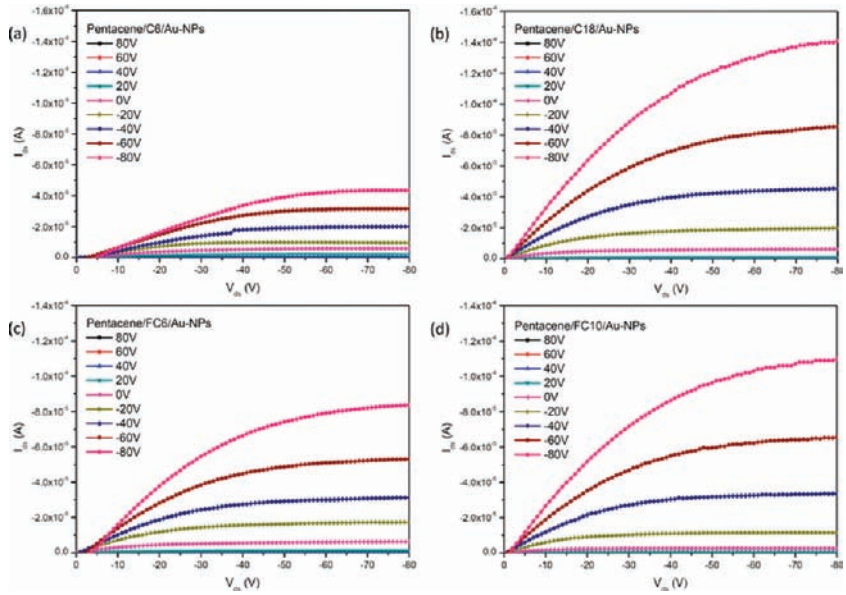

Figure 8. Output characteristics of the devices with various SAMs-modified Au NPs: (a) C6-Au-NPs, (b) C18-Au-NPs, (c) FC6-Au-NPs, and (d) FC10-Au-NPs.

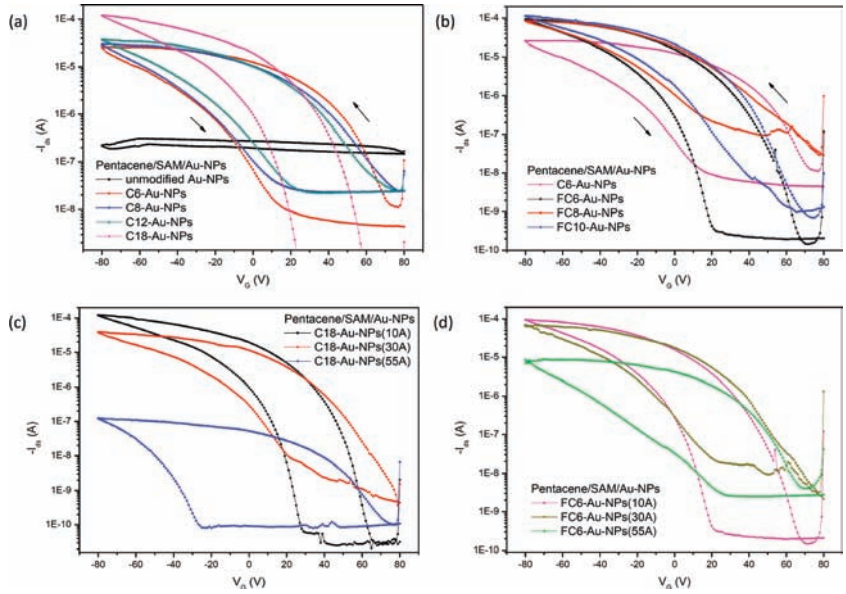

Figure 9. Transfer characteristics with bidirection scan gate voltage ranges for the devices. The V_{ds} was kept at −50 V, and the V_{gs} bias was swept from +80 to −80 V and returned to +80 V again: (a) devices with various C*n*-Au-NPs, (b) devices with C6-Au-NPs and various FC*n*-Au-NPs, (c) device of C18-Au-NPs of various particle sizes, (d) device of FC6-Au-NPs of various particle sizes. The arrows indicate the direction of the V_{gs} sweep. Each measurement was carried out with an integration time of 266 ms.

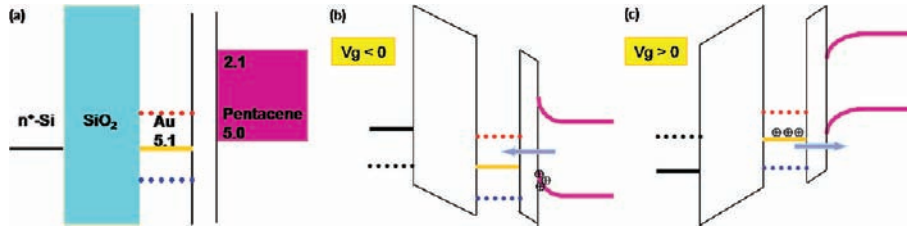

Figure 10. Schematic energy-band diagrams of pentacene/SAM/Au-NPs/silica/n^+-Si under (a) zero gate voltage, (b) program mode, and (c) erase mode. The red dotted line represents the work function for alkanethiol-modified Au, and the blue dotted line represents the work function for fluorinated alkanethiol-modified Au.

NPs. The results appear to correlate with the crystallinity results above such that with better crystallinity and large grain sizes of pentacene the mobility tends to be higher. The $I_{ds}-V_{ds}$ output curves of selected systems are shown in Figure 8.

Moreover, a clear hysteresis in the output current I_{ds} was observed as measured at a constant source−drain bias with the gate voltage swept between +80 and −80 V at a rate of 0.93 V s^{-1}. When the gate voltage was swept from +80 V toward the

Table 2. Device Characteristics as a Function of SAM Thiolate and Size of Au-NPs for the Organic FET/Memory Devices

	V_{th}			on−off	memory
	80 to −80 V	−80 to 80 V	mobility	ratio	window (V)
SiO_2	39.25	35.35	0.226	10^3	3.90
		Au(10 Å)-NPs surface			
unmodified Au(10)					
C6-Au	74.65	−6.35	0.036	10^4	81.00
C8-Au	62.11	−5.80	0.050	10^3	67.91
C12-Au	51.39	1.38	0.073	10^3	50.01
C18-Au	42.30	7.72	0.182	10^7	34.58
FC6-Au	39.45	−5.60	0.173	10^5	45.05
FC8-Au	42.01	2.00	0.182	10^3	40.01
FC10-Au	41.96	9.22	0.218	10^5	32.76
		Au(30 Å)-NPs surface			
C6-Au					
C18-Au	51.93	−4.24	0.068	10^5	56.17
FC6-Au	47.64	−9.31	0.130	10^4	56.95
		Au(55 Å)-NPs surface			
C6-Au					
C18-Au	67.34	−40.32	2.19×10^{-4}	10^4	107.66
FC6-Au	61.10	−20.55	0.018	10^3	81.65

negative direction, a trace of higher currents (high-conductivity state) was followed. When the gate voltage was swept from −80 V toward the positive direction, a trace of lower currents (low-conductivity state) was followed. This "electric bistability" behavior, that is, different conductivity at the same gate voltage, holds for all devices except the one with unmodified Au-NPs on the silica substrate, where no field-effect mobility was obtained. The I_{ds} curves as a function of the chain length used in capping the nanoparticles as well as the particle size are shown in Figure 9. Apparently there is a chain length effect as well as particle size effect in the hysteresis. The observed hysteresis is attributed to the charge-trapping effect of the Au-NPs embedded in the pentacene film since the reference devices without the Au-NPs had little such hysteresis.

A mechanism for the charge trapping is further suggested as follows. When a gate voltage is applied, charges accumulate in pentacene molecules at the dielectric/organic interface. The presence of Au-NPs affects the distribution of charges at this interface. Energy level alignment (Figure 10a) shows that the highest occupied molecular orbital (HOMO) level of pentacene (at ∼5.0 eV) is close to the work function of Au (5.1 eV).[14] With negative gate applied, the hole carriers induced in pentacene molecules at the interface can transfer into the Au-NPs and be trapped there (Figure 10b). The trapped hole charges in the Au-NPs form an internal electric field which partially offsets the external applied electric field, resulting in the low-conductivity state of the channel; this is called the programming process. On the other hand, with a positive bias applied, the hole charges can be detrapped from the Au-NPs to the surrounding pentacenes (Figure 10c). This is equivalent to the erasing process and results in the high-conductivity state.

The efficiency for the charges to be detrapped or trapped in the nanoparticles depends on the Schottky barrier at the metal/organic interface due to the mismatch of the work function of gold and the HOMO level of pentacene.[15] The presence of a self-assembled monolayer at the Au surface is known to modulate its work function as a result of the direction of the dipole interposed.[16−18] Fluorinated *n*-alkanethiol increases the work function of Au (to ∼5.5 eV) so that an increasing Schottky barrier exists for holes to transfer from pentacene to the Au-NPs (blue dotted line in Figure 10b) and a reduced barrier or even Ohmic contact results for holes to eject back to pentacene (blue dotted line in Figure 10c). On the other hand, *n*-alkanethiol monolayer lowers the work function of Au (to ∼4.5 eV) and facilitates the transport (and trapping) of hole charges from pentacene to Au-NPs (red dotted line in Figure 10b) but disfavors the ejection of holes back to pentacene (red dotted line in Figure 10c).[19]

The memory window, defined as the threshold voltage shift (ΔV_{th}) in the bisweeps of the gate voltage, signifies the ability of charge storage of the device. Here, the memory window clearly depends on the SAM used for capping the nanopaticles, as shown in Figure 9 and Table 2. Thus, for the same chain length SAM, charge storage is more facile for the *n*-alkanethiol-modified Au-NPs than the fluorinated thiol-modified Au-NPs and thus a larger memory window is expected. This is also what was observed (see Table 2). There is also a chain length effect within the same series of modification. The monolayer imposes a tunneling barrier which depends on the chain length of SAM-forming molecule.[20] The work functions of Au modified by *n*-alkanethiol of different chain lengths are similar (to within 0.1 eV for C6SH and C18SH) and so is the work function of Au modified by fluorinated alkanethiol of different chain lengths. The differentiating parameter will be the chain length. Longer chain SAM disfavors the charge transport from pentacene to Au-NPs, and the memory window is expected to be smaller. This explains the memory window changes from 81 to 34 V as the monolayer chain length changes from C6 to C18 (Table 2).

The particle size is also expected to affect the memory window. With the same capping monolayer, larger particles are expected to store more charges than smaller ones. This has been observed for both C18-Au-NPs and FC6-Au-NPs (Figure 9 and Table 2).

Having said that positive gate bias serves to expel the positive charges stored in the nanoparticles, we also cycled the gate voltages between −80 and 0 V after an initial scan of gate voltage from +80 to −80 V. This serves to charge the particles with holes in each cycle without discharging them with positive bias. There is a negative shift in V_{th}, more significant at the high-conductivity state than at the low-conductivity state, causing a reduced hysteresis (Figure 11). Repetitive scans brought about incremental shifts and eventually stabilized. Depending on the chain length of the SAM used, the ultimate $I-V$ characteristics are somewhat different. With C18-Au-NPs, the current and hysteresis decreased with repetitive sweeps to eventually a converged curve (Figure 11a). Thus, the repetitive sweeps between 0 and −80 V increase the positive charges in the nanoparticles to a final saturated state, and the charges did not get lost significantly during the sweeping from −80 to 0 V. On the other hand, with C6-Au-NPs, the hysteresis stabilized in the second sweep and remained nearly constant (Figure 11b). It is suggested that with shorter chain length the detrapping of positive charges (to reduce the repulsion between charges stored

(14) Briseno, A. L.; Mannsfeld, S. C. B.; Lu, X.; Xiong, Y.; Jenekhe, S. A.; Bao, Z.; Xia, Y. *Nano Lett.* **2008**, *93*, 053304.
(15) Tang, C. W. *Appl. Phys. Lett.* **1986**, *48*, 183.
(16) Crispin, X.; Geskin, V.; Crispin, A.; Cornil, J.; Lazzaroni, R.; Salaneck, W. R.; Bredas, J. L. *J. Am. Chem. Soc.* **2002**, *124*, 8131.
(17) Boer, B. D.; Hadipour, A.; Mandoc, M. M.; Woudenbergh, T. V.; Blom, P. W. M. *Adv. Mater.* **2005**, *17*, 621.
(18) Hung, M. C.; Wu, K. Y.; Tao, Y. T.; Huang, H. W. *Appl. Phys. Lett.* **2006**, *89*, 203106.
(19) Wu, K. Y.; Szu-Yen, Yu; Tao, Y. T. *Langmuir* **2009**, *25*, 2260–2266.
(20) Wu, K. Y.; Tao, Y. T. *Appl. Phys. Lett.* **2007**, *90*, 241104.

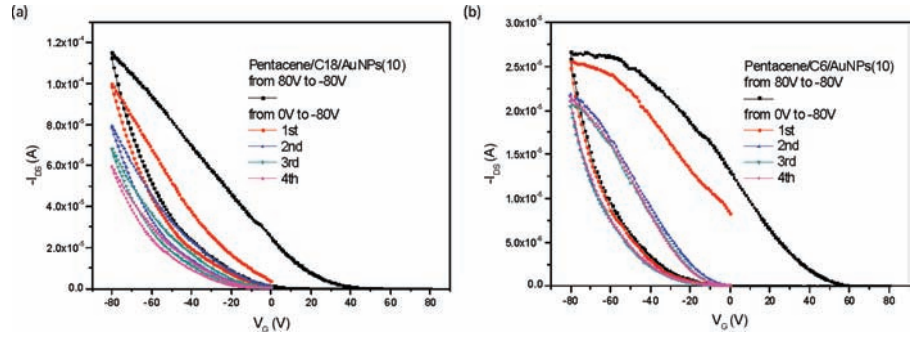

Figure 11. Transfer characteristics of a device based on (a) C18-Au-NPs and (b) C6-Au-NPs. The gate voltage was first applied from +80 to −80 V and then cycled between 0 and −80 V.

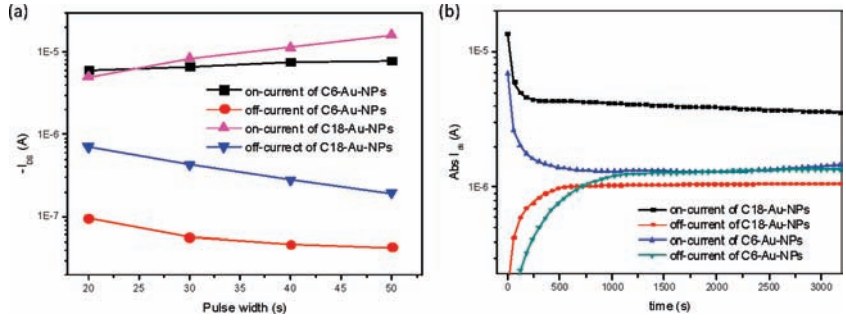

Figure 12. (a) Source−drain current as a function of gate pulse time at two devices based on C6- and C18-Au-NPs, respectively. The on and off current were measured at a constant $V_{ds} = -50$ V with the gate voltage kept at 0 V, after applying a 80 (erasing) and −80 V (programming) gate pulse. (b) Retention characteristics of the SAM-Au-NPs devices that were measured at $V_{ds} = -50$ V and $V_g = 0$ V after programming and erasing by applying a gate bias of −80 and 80 V for 50 s at $V_{ds} = 0$ V.

in the same particle) occurs to some extent when the gate bias is reduced toward 0 V. Thus, trapping of positive charges during sweep from 0 to −80 V and detrapping of positive charge during sweep from −80 to 0 V reaches a equilibrium after the second sweep. A finite hysteresis is maintained. The longer chain SAM, such as C18, better holds the charges, fewer and fewer hole charges can be injected into the particles in each additional scan toward −80 V, and litttle hole charges are lost during the scans toward 0 V. The hysteresis diminished. It should be noted that a voltage sweep to +80 V recovers the initial full hysteresis in both cases. These results indicate the device could be programmed (0 to −80 V) and erased (+80 to 0 V) repeatedly, but the memory is better kept with long alkyl chain SAM modification of the Au-NPs.

The on/off state of the transistor/memory device is triggered by the application of gate voltage and thus the trapping/detrapping of charges. The on/off ratio is determined by the amount of charges stored in the Au-NPs at the "off" state and the depletion of charges at the "on" state. It is a dynamic process depending on the gate voltage and the type and chain length of SAM modification. While the high-conduction (on) state and low-conduction (off) state can be achieved through bias sweep routines, they can also be obtained by a bias pulse. The device can be "turned on" by applying a +80 V gate voltage and "turned off" by applying a −80 V gate voltage and the currents measured at 0 V gate voltage under a constant source drain bias. The device with C6-Au-NPs gave a higher on/off ratio than the one with C18-Au-NPs, presumably because the charges are trapped and detrapped more readily for C6-Au-NPs. With the hydrocarbon chain as the tunneling barrier, it is expected that the on/off ratio may depend on the pulse time applied, more sensitive for the long chain thiol-modified Au-NPs case. Figure 12a shows the effect of the pulse time on the memory property of the devices. In the case of the device with C6-Au-NPs, the shorter program/erase pulse time resulted in a higher on/off ratio (∼100), which suggests the short alkyl-chain modification has a faster response to the switching action. For C18-Au-NPs, the on−off ratio increases with increasing pulse time because a longer pulse time is needed to store or remove charges from the particles.

Insomuch as chain length influences the efficiency of charge transfer into the particles, it also influences the retention of the charges once stored in the particles and thus the stability (lifetime) of the memory devices. Figure 12b shows the currents measured at 0 V gate voltage at a constant source−drain bias of −50 V, after the device was "turned on" at a pulse of 80 V for 50 s or "turned off" at a pulse of −80 V for 50 s. The device with C18-Au-NPs showed relatively slow decay in the on current and slow increase of the off current to a constant value which is around 20% of its initial value after around 1 h reading. However, relatively rapid decay occurred in the device for C6SH modification, with the on current equal to the off current after 1800 s. The fast rate of relaxation indicates the short alkyl chain allows rapid trapping and detrapping of the charge carriers in gold nanoparticles due to a low tunneling barrier.

Conclusion

We demonstrated an easy approach to embed Au-NPs into the conduction channel of a pentacene film-based field-effect transistor while maintaining the crystallinity and morphology of pentacene films needed for high-field-effect mobility for such films. Au-NPs capped with organic self-assembled monolayer serve as a floating gate through trapping carrier charges into the particles. The efficiency for the charges to be detrapped or kept in the nanoparticles depends on the character and chain length of the SAM-forming molecules

as well as the gold particle sizes. Hysteresis in the conductivity as a function of gate voltage was observed due to the trapped charges. The difference between the on-state current and off-state current (and thus the memory window) as a result of shifts in threshold voltages depends on the SAM used and can be tuned rationally. In general, a lower work function for the metal nanoparticle and smaller tunneling barrier contribute to the fast trapping and storing of hole charges in the nanoparticles. A larger tunneling barrier with long chain SAM slows down the trapping process but helps retain the charges. These understandings may provide grounds for further development of a practical transistor/memory device.

Acknowledgment. The authors thank the National Science Council of Taiwan, the Republic of China for financial support of this work.

JA904882M